Progress in PHOTOVOLTAICS

PROGRESS IN PHOTOVOLTAICS: RESEARCH AND APPLICATIONS
Prog. Photovolt: Res. Appl. (2017)
Published online in Wiley Online Library (wileyonlinelibrary.com). DOI: 10.1002/pip.2895

SHORT COMMUNICATION

InAlAs photovoltaic cell design for high device efficiency

Brittany L. Smith[1], Zachary S. Bittner[1], Staffan D. Hellstroem[1], George T. Nelson[1], Michael A. Slocum[1], Andrew G. Norman[2], David V. Forbes[1] and Seth M. Hubbard[1]*

[1] Rochester Institute of Technology, NanoPower Research Laboratory, 168 Lomb Memorial Drive, Rochester, NY, USA, 14623
[2] NREL, National Center for Photovoltaics, 15013 Denver West Parkway, Golden, CO, USA

ABSTRACT

This study presents a new design for a single-junction InAlAs solar cell, which reduces parasitic absorption losses from the low band-gap contact layer while maintaining a functional window layer by integrating a selective etch stop. The etch stop is then removed prior to depositing an anti-reflective coating. The final cell had a 17.9% efficiency under 1-sun AM1.5 with an anti-reflective coating. Minority carrier diffusion lengths were extracted from external quantum efficiency data using physics-based device simulation software yielding 170 nm in the n-type emitter and 4.6 μm in the p-type base, which is more than four times the diffusion length previously reported for a p-type InAlAs base. This report represents significant progress towards a high-performance InAlAs top cell for a triple-junction design lattice-matched to InP. Copyright © 2017 John Wiley & Sons, Ltd.

KEYWORDS
InAlAs; InP; MOVPE; multijunction solar cell

***Correspondence**
Seth Hubbard, Rochester Institute of Technology, 168 Lomb Memorial Drive, Rochester, New York, 14623 USA.
E-mail: smhsps@rit.edu

Received 14 September 2016; Revised 9 March 2017; Accepted 20 March 2017

1. INTRODUCTION

InAlAs has conventionally been used as a wide-bandgap barrier material in optoelectronics lattice-matched to InP because of its 1.45 eV bandgap; however, it has undergone little development for photovoltaic applications [1,2]. A small number of InAlAs photovoltaic cells have been studied to date, including $In_{0.52}Al_{0.48}As$ lattice-matched to InP, $In_{0.52}Al_{0.48}As$ cell grown on metamorphic grading on a GaAs substrate, and $In_{0.37}Al_{0.63}As$ grown on an engineered substrate [3–5]. When lattice-matched to InP, band parameters predict $In_{0.52}Al_{0.48}As$ to have a bandgap of 1.437 eV, although it has been reported to vary up to 100 meV [6,7]. This material could comprise the top cell of an all-lattice-matched InP-based triple junction device; however, the maximum efficiency of an InAlAs/InGaAsP/InGaAs (1.5 eV/1.1 eV/0.7 eV) device is only 26.5% under 1 sun AM1.5 [8]. In order to increase efficiency, the top-cell bandgap must be increased into the 1.7–1.8 eV range. Adding antimony, the quaternary alloy $In_{0.21}Al_{0.79}As_{0.74}Sb_{0.26}$ has a direct bandgap of 1.74 eV and is lattice-matched to InP [9]. A triple junction cell with InAlAsSb/InGaAsP/InGaAs (1.74 eV/1.17 eV/0.7 eV) subcells lattice-matched to InP could achieve up to 52.8% under 500 suns AM1.5 [10]. Furthermore, $In_{0.37}Al_{0.63}As$ lattice-matched to an engineered substrate with a lattice constant of 5.80 Å has a bandgap of 1.93 eV [5]. This substrate has been experimentally demonstrated by growing a strained layer of InGaAs with a 5.80 Å lattice constant on InP, then removing the InP substrate and transferring the InGaAs layer to a glass substrate [5]. This virtual substrate can then be used as a crystalline template on which to grow a triple junction cell. The proposed triple junction InAlAs/InGaAsP/InGaAs (1.93 eV/1.39 eV/0.94 eV) is predicted to have an efficiency of 40.4% under 1-sun AM1.5 and 51.8% under 100-suns [11].

Development of InAlAs lattice-matched to InP is a useful starting point to develop InAlAsSb lattice-matched to InP as well as InAlAs with alternative lattice constants. So far, experimental reports have demonstrated 14.2% efficiency under 1-sun AM1.5 for a single junction $In_{0.52}Al_{0.48}As$ cell latticed-matched to InP, and 5% efficiency under 1-sun AM1.5 for a single-junction $In_{0.52}Al_{0.48}As$ cell grown on a metamorphic grading on a

Copyright © 2017 John Wiley & Sons, Ltd.

Pursuant to the DOE Public Access Plan, this document represents the authors' peer-reviewed, accepted manuscript. The published version of the article is available from the relevant publisher.

GaAs substrate [3,4]. The research presented in this publication is a step further towards realizing InAlAs as a useful top cell in multi-junction designs. Sentaurus Device™ (a physics-based finite-element device simulation package by Synopsys, Inc.) was used to optimize a device design based on inputs from literature as well as bulk InAlAs layers grown for the study. This article first presents design parameters for the InAlAs cell and its predicted performance based on simulation. Devices were grown by metal organic vapor phase epitaxy (MOVPE), which is known to produce higher material quality InAlAs than molecular beam epitaxy even though molecular beam epitaxy is more commonly used to grow InAlAs [12]. Fits to experimental data using the Sentaurus Device™ software were used to extract device parameters. Finally, an improved cell efficiency under 1-sun AM1.5 is presented.

2. THEORY AND SOLAR CELL DESIGN

Initial design considerations focused on comparing InAlAs cells from literature. The highest performing cell was an n-on-p device with a 200 nm emitter and a 1500 nm base, with extracted lifetimes used for simulations in Table I [4]. Bulk layers of doped InAlAs were grown by MOVPE to inform cell design, and results from Hall effect measurements are also shown in Table I. Thicknesses for the final design were determined based on these mobilities and other parameters in Table I, by iterative simulations using a one-dimensional minority carrier drift/diffusion model [4,16]. The optimized cell structure is shown in Figure 1(a). A 50 nm intrinsic region (i-region) was included between the emitter and base in order to prevent dopant diffusion and compensation.

Table I. Input parameters for cell design simulations.

Parameter	Value	Reference
4.5×10^{17} cm^{-3} p-InAlAs hole mobility	27 cm^2 V^{-1} s^{-1}	measured
2×10^{18} cm^{-3} n-InAlAs electron mobility	905 cm^2 V^{-1} s^{-1}	measured
Emitter minority carrier lifetime – holes (extracted from EQE)	400 picoseconds	[4]
Base minority carrier lifetime – electrons (extracted from EQE)	4 nanoseconds	[4]
n, k optical constants	See reference	[13]
Front surface recombination velocity	1×10^6 cm/s	[14]
Window/emitter interface surface recombination velocity	200 cm/s	[15]
Rear surface recombination velocity	5000 cm/s	[14]

EQE, external quantum efficiency.

Strained InAlAs was selected for the top window because of the limited availability of high bandgap InP lattice-matched materials. Alternatives include AlAsSb or InAlAsSb; however, these materials need further material development before they can be grown at high quality by MOVPE and do not offer as large of a valence band offset as strained InAlAs [15]. The strained $In_{0.35}Al_{0.65}As$ window is predicted to have a bandgap of 1.754 eV via interpolation of parameters reported by Vurgaftman *et al.*,

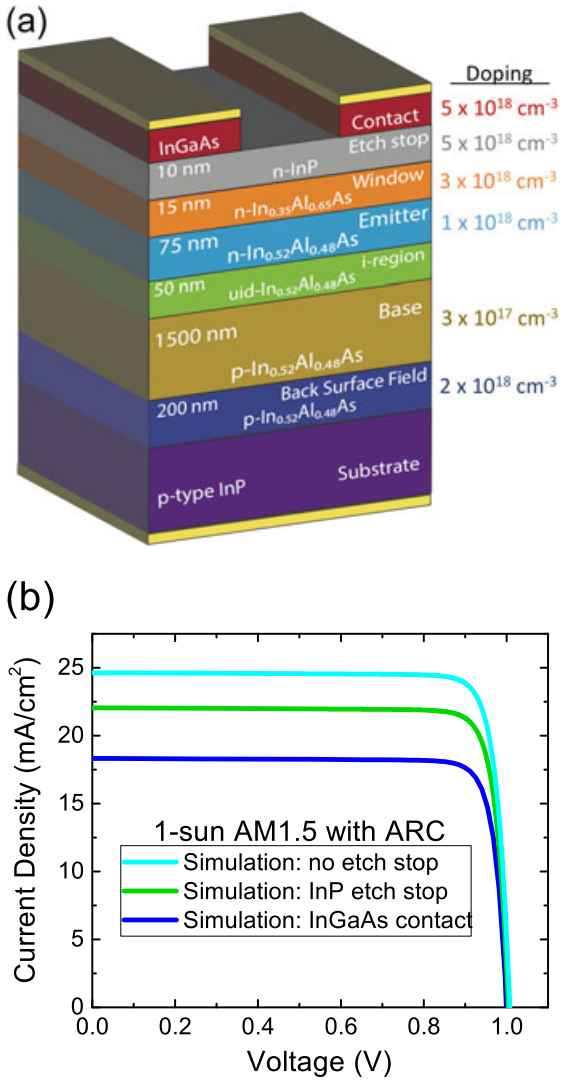

Figure 1. (a) Schematic of single-junction InAlAs device design with InGaAs underneath metal only. **(b)** Simulated light I–V results of InAlAs cells with low trap density to establish a benchmark of 'ideal' performance: 'InGaAs contact' has no InP etch stop but retains the 20 nm InGaAs contact layer between grid fingers, 'InP etch stop' removes the 20 nm InGaAs contact between grid fingers but retains the 10 nm InP etch stop (exact schematic in Figure 1(a)), and 'No etch stop' has neither InGaAs nor InP between the grid fingers. ARC, anti-reflective coating. [Colour figure can be viewed at wileyonlinelibrary.com]

Prog. Photovolt: Res. Appl. (2017) © 2017 John Wiley & Sons, Ltd.
DOI: 10.1002/pip

Pursuant to the DOE Public Access Plan, this document represents the authors' peer-reviewed, accepted manuscript. The published version of the article is available from the relevant publisher.

accounting for bowing and strain shifts [7]. The interpolation indicates that the conduction band of the $In_{0.35}Al_{0.65}As$ window is offset from the conduction band of the emitter by 256 meV, and the valence band is offset by 61 meV. This is an adequate barrier for holes in the window layer given that the emitter is n-type, and the electric field of 17.6 kV/cm in the window layer acts as passivation. Because the selected window is strained, defects could potentially occur in the window/emitter interface. Such defects would increase the surface recombination velocity (SRV), which degrades quantum efficiency. Defects may occur once the critical thickness of a strained layer is exceeded, and the layer begins to relax. The maximum critical thickness for the nominal material is 9.1 nm as predicted by Mathews and Blakeslee [17]. Given that the Mathews-Blakeslee limit is known to produce conservative estimates of critical thickness, and the window layer is on the order of the critical thickness, it can be assumed that the window is in the pseudomorphic regime, and the density of misfit dislocations at the interface is low. Previous work on an $In_{0.3}Al_{0.7}As$ window for InP-based materials reported an SRV below 200 cm/s, which indicates defects are not excessive [15]. In order to prevent defect formation in the optically active regions of the cell, $In_{0.52}Al_{0.48}As$ with a doping of 2×10^{18} cm^{-3} was employed as a back surface field between the base and the substrate rather than a strained rear window.

Because previous reports were unable to remove the contact layer without degrading cell performance because of rapid oxidation of the high-aluminium content window, an InP etch stop layer was added to the design to protect the window [18]. One could conceivably etch the contact layer and attempt to deposit an anti-reflective coating (ARC) immediately to minimize window oxidation, although some oxidation may still occur. However, incorporating an InP etch stop into the design permits the selective etch of the contact layer without exposing the window. To quantify the improvement from reducing absorption losses, the simulation of a device retaining the 20 nm InGaAs contact layer was compared with the simulation of a device with an InP etch stop, and also compared with a device with neither contact layer nor etch stop. Sentaurus Device™ was used to simulate AM1.5G I-V performance. The simulations used most parameters from Table I except minority carrier lifetimes. Lifetimes were calculated from the electron effective mass in InAlAs and a mid-gap electron trap with low density (1×10^{14} cm^{-3}) to approximate a high quality cell, which corresponded to lifetimes on the order of 80 nanoseconds [13,19]. Front surface recombination velocity was held constant for all simulations as a reasonable approximation for a front SRV. Figure 1(b) shows light I–V simulations comparing devices with a top layer of either 20 nm InGaAs, 10 nm InP, or 15 nm $In_{0.35}Al_{0.65}As$, each with an optimized Si_3N_4 anti-reflective coating. The short-circuit current (J_{sc}) for a device with an InGaAs cap is 18.3 mA/cm^2, while the InP cap has a J_{sc} of 22.1 mA/cm^2, and the device with the exposed $In_{0.35}Al_{0.65}As$ window has a J_{sc} of 24.6 mA/cm^2. This represents a 21% relative increase in efficiency when using an InP cap rather than InGaAs, and an 11% increase when removing the InP cap from the $In_{0.35}Al_{0.65}As$ window. These simulation results confirm that it is advantageous to remove the InGaAs layer and include the InP etch stop in order to protect the high-aluminium content window from oxidation. Furthermore, the simulation results with the InP etch stop can serve as an ideal performance benchmark for the design in Figure 1(a), with a J_{sc} of 22.1 mA/cm^2, an open-circuit voltage (V_{oc}) of 1.00 V, and an efficiency of 19.2% under 1-sun AM1.5G with an 87% fill factor. Removing the InP etch stop immediately before depositing the ARC could improve the device performance further, representing another 11% increase in 1-sun AM1.5G efficiency of 21.4%.

3. EXPERIMENTAL

InAlAs solar cells were grown on two InP substrates in a Veeco D125 3 × 2" MOVPE reactor at 60 torr using a rotation of 1000 rpm. The metalorganic precursors were trimethylindium, trimethylaluminum, and arsine, doped with disilane for n-type and diethylzinc for p-type. Trimethylindium was flowed at a rate of 39.4 μmol/min, trimethylaluminum at 35.5 μmol/min, and arsine at 1020 μmol/min, which corresponds to a V/III ratio of 100 and resulted in a growth rate of 1.94 μm/hr. The emitter was grown at 610 °C because silicon incorporation in InAlAs decreases significantly with temperature, whereas the base was grown at 580 °C in order to maintain p-dopant control. Layer thicknesses in the cells were verified by secondary-ion mass spectrometry as well as transmission electron microscopy. Devices were grown on InP:Zn (100) oriented substrates with a 2° offcut towards (110). Solar cells were fabricated using Au/Zn/Au as the p-type contact and Au/Ge/Ni/Au as the n-type contact. Cells were 1 cm × 1 cm with a grid finger spacing of 500 μm and 4% grid shadowing.

A 1 : 1 : 38 mixture of H_3PO_4:H_2O_2:H_2O was used as a mesa-etchant as well as a contact etchant because it does not etch InP and also results in more uniform InAlAs sidewalls than HCl-based etchants. The mesa was etched approximately 700 nm into the base in order to isolate the junction. A 1 : 1 : 2 mixture of HCl:H_3PO_4:CH_3COOH (acetic acid) was used as a selective etchant of the InP etch stop layer, with the acetic acid acting to dilute the etchant to increase etch uniformity and precision for the thin etch stop. This etchant exhibited 6 : 1 selectivity to InP over $In_{0.52}Al_{0.48}As$. This etchant was used to selectively remove the InP etch stop on one of the substrates immediately before depositing an ARC. A dual-layer ZnS/MgF_2 ARC was deposited by thermal evaporation, using 46 nm/97 nm, respectively, for the cells retaining the InP etch stop, and 49 nm/107 nm, respectively, for the cell with the etch stop selectively

Pursuant to the DOE Public Access Plan, this document represents the authors' peer-reviewed, accepted manuscript.
The published version of the article is available from the relevant publisher.

removed. The thicknesses for the ARC were optimized using the optical software TFCalc by minimizing reflectance in the wavelength range of interest (below the nominal bandgap of InAlAs) given the optical constants of the topmost layers (InP and $In_{0.35}Al_{0.65}As$, respectively) [20]. A photograph of a final device after ARC deposition is shown in Figure 2.

High resolution x-ray diffraction (HRXRD) of the solar cell was measured, and the data can be viewed in the supporting information for this article. HRXRD from the window layer indicates a composition of $In_{0.34}Al_{0.66}As$, which is a slight deviation from the nominal design, but is expected to have little impact overall. HRXRD of the solar cell indicates that the base was compressively strained by 620 ppm to the substrate, which corresponds to a slightly In-rich layer consisting of $In_{0.53}Al_{0.47}As$. The composition-dependent bandgap relation for InAlAs indicates such an alloy should have a bandgap of 1.42 eV [7]. Electroluminescence data is also available as supporting information and shows a peak at 1.40 eV, which is lower than expected and may include low-energy emission from the base, which was grown at a lower temperature. InAlAs grown below 615 °C is known to exhibit significant phase separation, where InAs-rich and AlAs-rich regions occur separately in the epilayer and can lower the bandgap as much as 290 meV [21]. This worsens as growth temperature decreases; therefore, the base grown at 580 °C would likely show a greater degree of phase separation than the emitter, which was grown at 610 °C. Furthermore, atomic ordering reported in InAlAs is also associated with bandgap reduction, although to a lesser degree [21,22]. In order to determine if these phenomena occur in the InAlAs epitaxial layers in this study, orthogonal <110> cross-sectional transmission electron microscopy (TEM) samples were prepared using mechanical polishing and 4 kV $argon^+$ ion milling (with the sample cooled using liquid nitrogen) for TEM analysis in an FEI Tecnai $G^2$30 SuperTwin TEM operated at 300 kV. A [110] cross-sectional (−220) dark-field TEM image and diffraction pattern are shown in Figure 3. The diffraction pattern in Figure 3(a) indicates weak atomic ordering on {111}B planes through the presence of weak ½{111} superlattice diffraction spots. The (−220) dark field TEM image in Figure 3(b) shows strain contrast corresponding to a compositional fluctuation on the 100 nm scale, which indicates a significant degree of phase separation is occurring in the sample. It is postulated that a combination of these effects is the cause of the 20 meV discrepancy between the electroluminescence peak as compared with the nominal bandgap estimate from HRXRD, and this will correspond to a 20 meV reduction in the open-circuit voltage of the device.

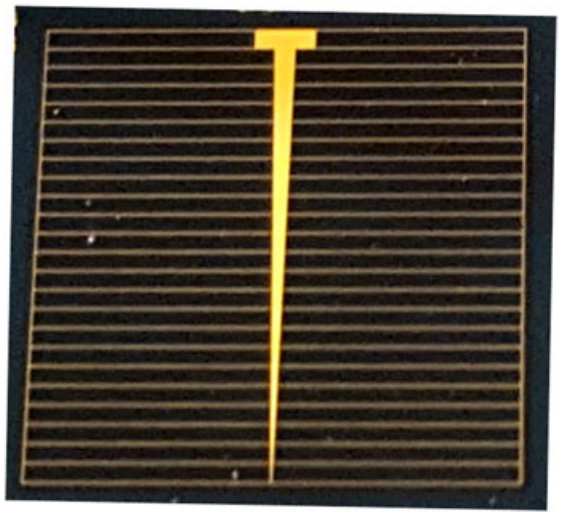

Figure 2. Photograph of fabricated 1 × 1 cm^2 InAlAs solar cell with anti-reflective coating. [Colour figure can be viewed at wileyonlinelibrary.com]

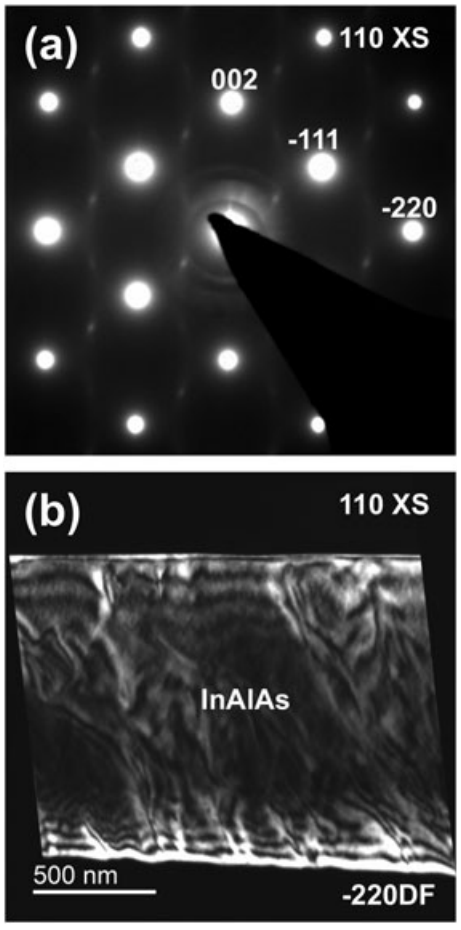

Figure 3. (a) [110] cross-sectional transmission electron diffraction pattern showing weak ½{111} superlattice spots arising from atomic ordering on {111}B planes. **(b)** dark-field image of [110] cross-section using (−220) reflection, where strain contrast features indicate compositional fluctuation in the alloy on the 100 nm scale.

Pursuant to the DOE Public Access Plan, this document represents the authors' peer-reviewed, accepted manuscript. The published version of the article is available from the relevant publisher.

4. RESULTS AND DISCUSSION

Experimental light I–V results under 1 sun AM1.5G illumination are shown in Figure 4 and summarized in Table II. Light I–V was measured in a two-zone TS Space Systems solar simulator calibrated with $InGaP_2$ and GaAs reference cells, which were calibrated to AM1.5G by the National Renewable Energy Laboratory. The AM1.5G spectrum was selected in order to permit comparison with cell results published in previous reports [3,4]. A total of seven cells were measured on the two wafers. Light I–V of the best performing cell from each wafer is shown in Figure 4(a). The best cell from the wafer that retained the InP etch stop had an efficiency of 17.1% under 1-sun AM1.5G. The average efficiency for the wafer was 16.7% with a standard deviation of 0.5%. The best cell from the wafer that had the InP etch stop selectively removed had an efficiency of 17.9% under 1-sun AM1.5G. The average efficiency for the wafer was 17.2% with a standard deviation of 0.5%. The reflectivity of the ARC is not identical between the two wafers because of non-uniformity in ZnS deposition, resulting in higher reflectance from the cell with the InP etch stop. However, a simple calculation confirms that if the reflectivity of the two wafers were identical, the cell without the etch stop would still exhibit 4% higher current. This is also evident in the internal quantum efficiency data, shown later in Figure 5(b).

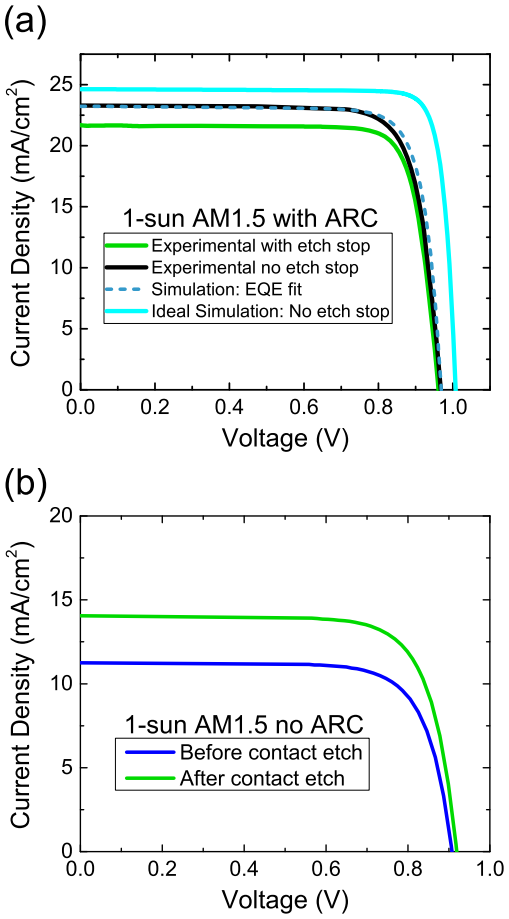

Figure 4. **(a)** Experimental light I–V of best performing cells, a simulated fit to experimental light I–V from best cell with no etch stop generated using lifetimes extracted from a fit to experimental external quantum efficiency data, and the 'benchmark' simulated light I–V curve shown in Figure 1 with no InP etch stop. **(b)** Experimental light I–V results from a cell before and after contact etch agree with predicted 21% J_{SC} increase. ARC, anti-reflective coating. [Colour figure can be viewed at wileyonlinelibrary.com]

Figure 4(a) includes two simulated IV curves, one is the ideal simulation of an InAlAs cell with no etch stop as shown in Figure 1(b), while the other simulation is intended to be a fit to experimental data from the best cell with no InP etch stop. The Light I–V fit was generated using the fit parameters reported in Table III and assumed an InAlAs bandgap of 1.437 eV in order to approximate the band edge seen in the EQE. Experimental light I-V measurements of a different cell on a wafer that retained the InP etch stop are shown in Figure 4(b) before and after contact etch without an ARC. This illustrates that the contact etch results in a 24% relative increase in J_{SC}, which is consistent with the current enhancement predicted via simulation in Figure 1(b).

External quantum efficiency data from the best cell without an etch stop is presented in Figure 5(a). Losses at short wavelengths are not excessive, which indicates the strained window is successfully passivated. At long wavelengths, the EQE extends roughly 70 nm past the band edge. The presence of this tail is assumed to be an effect of phase separation and atomic ordering in the base as described in the experimental section [21,22]. Figure 5 (a) also shows a fit to the EQE data, where minority carrier

Table II. Experimental light I–V results compared with simulation.

	J_{sc} (mA/cm^2)	V_{oc} (V)	FF (%)	Efficiency (%)
Best cell without etch stop (ARC)	23.3	0.97	79	17.9
Best cell with etch stop (ARC)	21.7	0.96	82	17.1
EQE fit simulation (ARC)	23.2	0.97	81	18.3
Ideal simulation without etch stop (ARC)	24.6	1.00	87	21.4
Before contact etch (no ARC)	11.3	0.91	75	7.7
After contact etch (no ARC)	14	0.92	75	9.7

ARC, anti-reflective coating; EQE, external quantum efficiency.

Pursuant to the DOE Public Access Plan, this document represents the authors' peer-reviewed, accepted manuscript.
The published version of the article is available from the relevant publisher.

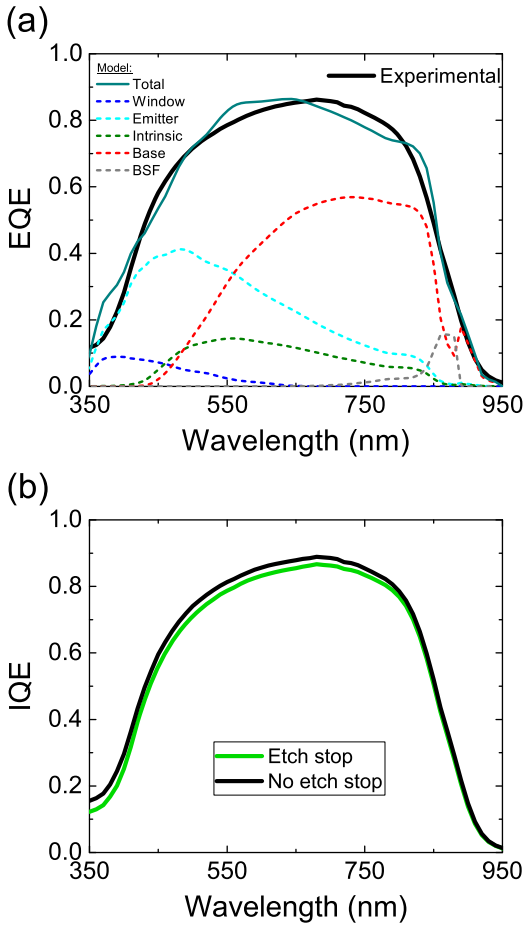

Figure 5. (a) Experimental external quantum efficiency data from best performing cell with no etch stop (with anti-reflective coating (ARC)) and simulated fit to external quantum efficiency data generated by adjusting lifetimes to approximate experimental results. The simulated fit used minority carrier lifetimes of 0.4 ns in the emitter and 9 ns in the base. Individual layer contributions of simulated fit are shown as dashed lines. **(b)** Internal quantum efficiency (IQE) data from the best cell of each of the two wafers: enhanced short wavelength response is observed upon etch stop removal. BSF, back surface field. [Colour figure can be viewed at wileyonlinelibrary.com]

Table III. Fit parameters for experimental device results.

Parameters	Values
Layer thicknesses	Figure 1(a)
Dopant concentrations	Figure 1(a)
Hole mobility	27 $cm^2\ V^{-1}\ s^{-1}$
Electron mobility	905 $cm^2\ V^{-1}\ s^{-1}$
Emitter minority carrier lifetime – holes	400 picoseconds
Base minority carrier lifetime – electrons	9 nanoseconds
Front surface recombination velocity	1×10^6 cm/s
Window/emitter interface surface recombination velocity	200 cm/s
Rear surface recombination velocity	5000 cm/s

lifetimes were adjusted in the device simulation software Sentaurus to approximate the experimental data and are reported in Table III. The front and rear SRV were determined based on reference [14], while the window/emitter interface SRV was based on reference [15]. The fit used minority carrier lifetimes of 400 ps in the emitter and 9 ns in the base, which correspond to minority carrier diffusion lengths of 170 nm and 4.6 µm, respectively, although the diffusion length calculated for the base is slightly overestimated because of EQE tailing. In order to fit the experimental data, a bandgap of 1.437 eV defined within the model provided a reasonable approximation of both the current collection observed near the band edge and the open circuit voltage as shown in Figure 4(a). In order to approximate the experimentally observed band tailing in the model, the extinction coefficient used for InAlAs was iteratively increased above the band gap. The internal quantum efficiency data shown in Figure 5(b) illustrates the inherent device improvement when removing the InP etch stop, regardless of ARC efficacy.

The minority carrier lifetime extracted from the base Figure 5(a) differs from the lifetime used when initially designing the device, which was determined from the reference in Table I. Using the lifetimes from Figure 5(a) as inputs, simulations indicate that using a 3.5 µm base would be 19% efficient under AM1.5G with an ARC and no etch stop. This would be directly achievable given that the material quality and the ability to deposit an ARC immediately after removing the etch stop to prevent oxidation of the window have both already been demonstrated in this study. An experimental demonstration of this re-optimized cell design would further establish InAlAs as a qualified option for the top-cell applications described in the introduction.

Dark current–voltage (dark I–V) and J_{sc}-V_{oc} data are shown in Figure 6. A fit to a two-diode equation

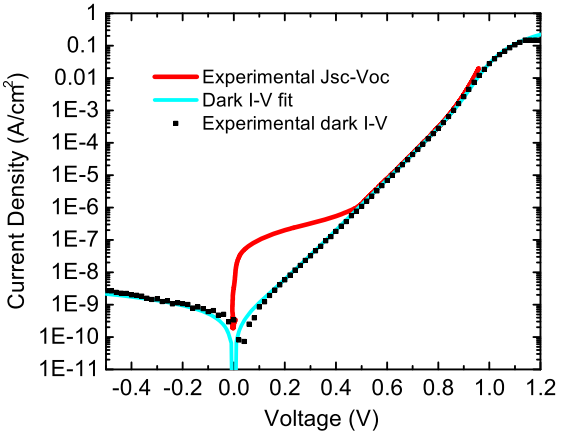

Figure 6. Experimental and fitted dark I–V data using a two-diode model where $J_{01} = 7.8 \times 10^{-19}$ A/cm^2, and experimental J_{SC}-V_{OC} data to extract series and shunt resistance. [Colour figure can be viewed at wileyonlinelibrary.com]

Prog. Photovolt: Res. Appl. (2017) © 2017 John Wiley & Sons, Ltd.
DOI: 10.1002/pip

Pursuant to the DOE Public Access Plan, this document represents the authors' peer-reviewed, accepted manuscript. The published version of the article is available from the relevant publisher.

(Equation (1)) indicates ideality factors (n) of 1 and 2.15, respectively. The n = 1 region occurs near the reported Voc which implies even at 1-sun the device is beginning to operate in the radiatively limited regime. The extracted dark series resistance was 0.74 ohms/cm^2, and the shunt resistance was 2.0×10^8 ohms/cm^2. Series resistance was also calculated using the J_{SC}-V_{OC} and light I–V data as published in [23], which corresponds to a 1-sun illuminated series resistance of 1.25 ohms/cm^2. The series resistance is higher than desired and could be reduced by increasing the thickness of the grid fingers. The shunt resistance value is notably high, comparable with other well-developed III–V devices such as GaAs, which implies that there are few bulk defects occurring in the epitaxial layers. The dark currents for this fit were $J_{01} = 7.8 \times 10^{-19}$ A/cm^2 and $J_{02} = 1.5 \times 10^{-10}$ A/cm^2, respectively. An ideal J_{01} for InAlAs calculated from experimental mobility values and bandgap, nominal doping, effective masses from literature, and the diffusion lengths extracted earlier is 8.6×10^{-20} A/cm^2. The experimental J_{01} is less than an order of magnitude greater than this value and would improve with material quality. Furthermore, the experimental dark current density is two orders of magnitude greater than typically seen from the highest performing GaAs solar cells, which implies the InAlAs material quality has room for improvement compared with well-developed III–V materials [24].

$$J_{dark} = J_{01}\left(e^{\frac{q\left(V-JR_{series}\right)}{n_1 kT}} - 1\right) + J_{02}\left(e^{\frac{q\left(V-JR_{series}\right)}{n_2 kT}} - 1\right) + \frac{V - JR_{series}}{R_{shunt}} \quad (1)$$

5. CONCLUSIONS

This study has successfully presented a high efficiency design for single-junction InAlAs solar cells. This cell represents an improvement on previous studies by reducing parasitic absorption losses from the low band-gap contact layer while maintaining a functional window layer by integrating a selective etch stop layer, which is removed immediately before depositing an anti-reflective coating. Furthermore, the minority carrier diffusion lengths extracted from EQE data are more than 1.5 times the thickness of their respective layers, which results in good collection. The cell presented in this study has achieved 17.9% efficiency under 1-sun AM1.5 for these reasons, which represents a significant improvement over previously published single-junction $In_{0.52}Al_{0.48}As$ efficiencies. Further development of this technology could utilize a cell design optimized for the minority carrier lifetimes reported in this study to achieve 19% efficiency and should consider the effects of phase separation and atomic ordering on the InAlAs bandgap when selecting growth temperature.

ACKNOWLEDGEMENTS

This work was supported by the Advanced Research Projects Agency – Energy: Grant #DE-AR0000335, NASA Space Technology Research Fellowship NNX15AP53H, and the US Department of Energy under Contract DE-AC36-08GO28308 with the National Renewable Energy Laboratory. The author of this work would like to thank collaborators at the Naval Research Laboratory and Microlink Devices for information on the materials system and the NASA Space Act Agreement SAA3-844-3 for use of the MOVPE reactor for material growth.

REFERENCES

1. Fujita S, Noda T, Nozaki C, Ashizawa Y. InGaAs/InAlAs HEMT with a strained InGaP Schottky contact layer. *IEEE Electron Device Letters* 1993; **14**(5): 259–261 https://doi.org/10.1109/55.215186.
2. Lenox C, Nie H, Yuan P, Kinsey G, Homles AL Jr, Streetman BG, Campbell JC. Resonant-cavity InGaAs-InAlAs avalanche photodiodes with gain-bandwidth product of 290 GHz. *IEEE Photonics Technology Letters* 1999; **11**(9): 1162–1164 https://doi.org/10.1109/68.784238.
3. Mathews I, O'Mahony D, Gocalinska A, Manganaro M, Pelucchi E, Schmidt M, Morrison AP, Corbett B. InAlAs solar cell on a GaAs substrate employing a graded InxGa1− xAs–InP metamorphic buffer layer. *Applied Physics Letters* 2013; **102**(3): 033906–4 https://doi.org/10.1063/1.4789521.
4. Leite MS, Woo RL, Hong WD, Law DC, Atwater HA. Wide-band-gap InAlAs solar cell for an alternative multijunction approach. *Applied Physics Letters* 2011; **98**(9): 093502–3 https://doi.org/10.1063/1.3531756.
5. Leite MS, Warmann EC, Kimball GM, Burgos SP, Callahan DM, Atwater HA. Wafer-scale strain engineering of ultrathin semiconductor crystalline layers. *Advanced Materials* 2011; **23**(33): 3801–3807 https://doi.org/10.1002/adma.201101309.
6. Wakefield B, Halliwell MAG, Kerr T, Andrews DA, Davies GJ, Wood DR. Direct energy gap of Al1−xInxAs lattice matched to InP. *Applied Physics Letters* 1984; **44**(3): 341–343 https://doi.org/10.1063/1.94726.
7. Vurgaftman I, Meyer J, Ram-Mohan L. Band parameters for III–V compound semiconductors and their alloys. *Journal of Applied Physics* 2001; **89**(11): 5815–5875 https://doi.org/10.1063/1.1368156.
8. Woo RL, Hong WD, Mesropian S, Leite MS, Atwater HA, Law DC. First demonstration of monolithic InP-based InAlAs/InGaAsP/InGaAs triple junction solar cells. *37th IEEE Photovoltaic Specialists*

Pursuant to the DOE Public Access Plan, this document represents the authors' peer-reviewed, accepted manuscript. The published version of the article is available from the relevant publisher.

Conference, 2011. IEEE, https://doi.org/10.1109/PVSC.2011.6185903.
9. Lumb MP, Gonzalez M, Vurgaftman I, Meyer JR, Abell J, Yakes M, Hoheisel R, Tischler JG, Jenkins PP, Stavrinou PN. Simulation of novel InAlAsSb solar cells. SPIE OPTO; 2012: International Society for Optics and Photonics, https://doi.org/10.1117/12.909324.
10. González M, Chan N, Ekins-Daukes NJ, Adams JGJ, Stavrinou P, Vurgaftman I, Meyer JR, Abell J, Walters RJ, Cress CD, Jenkins PP. Modeling and analysis of multijunction solar cells. SPIE, the International Society for Optical Engineering; San Francisco 2011. p. 79330R–R-12, https://doi.org/10.1117/12.875757.
11. Leite MS, Woo RL, Munday JN, Hong WD, Mesropian S, Law DC, Atwater HA. Towards an optimized all lattice-matched InAlAs/InGaAsP/InGaAs multijunction solar cell with efficiency >50%. *Applied Physics Letters* 2013; **102**(3): 033901–5 https://doi.org/10.1063/1.4758300.
12. Luo JK, Thomas H, Clark SA, Williams RH. The effect of growth temperature on the electrical properties of AlInAs/InP grown by molecular beam epitaxy and metal-organic chemical-vapor deposition. *Journal of Applied Physics* 1993; **74**(11): 6726–6733 https://doi.org/10.1063/1.355069.
13. Matthews J, Blakeslee A. Defects in epitaxial multilayers: I. Misfit dislocations. *Journal of Crystal Growth* 1974; **27**: 118–125 https://doi.org/10.1016/S0022-0248(74)80055-2.
14. Norman AG, Mallard RE, Murgatroyd IJ, Booker GR, Moore AH, Scott MD. TED, TEM and HREM studies of atomic ordering in $Al_xIn_{1-x}As$ epitaxial layers grown by OMVPE. *Institute of Physics Conference Series* 1987; **87**: 77–82.
15. Dinges H, Burkhard H, Lösch R, Nickel H, Schlapp W. Refractive indices of InAlAs and InGaAs/InP from 250 to 1900 nm determined by spectroscopic ellipsometry. *Applied Surface Science* 1992; **54**: 477–481 https://doi.org/10.1016/0169-4332(92)90090-K.
16. Hovel H. The effect of depletion region recombination currents on the efficiencies of Si and GaAs solar cells. *10th IEEE Photovoltaic Specialists Conference*, IEEE Palo Alto, Calif, 1974.
17. Bothra S, Tyagi S, Ghandhi SK, Borrego JM. Surface recombination velocity and lifetime in InP. *Solid-State Electronics* 1991; **34**: 47–50 https://doi.org/10.1016/0038-1101(91)90199-9.
18. Yakes MK, Schmieder KJ, Lumb MP, Bennett MF, Gonzalez M, Cunningham PD, Khachatrian A, Hirst LC, Tomasulo S, Kotulak NA, editors. Evaluation of strained InAlAs as a window layer for wide bandgap materials lattice matched to InP. *42nd IEEE Photovoltaic Specialist Conference*, IEEE, 2015.
19. Leite MS, Woo RL, Hong WD, Law DC, Atwater HA, editors. InAlAs epitaxial growth for wide band gap solar cells. *37th IEEE Photovoltaic Specialists Conference*, IEEE, 2011, https://doi.org/10.1109/PVSC.2011.6186070.
20. Olego D, Chang T, Silberg E, Caridi E, Pinczuk A. Compositional dependence of band-gap energy and conduction-band effective mass of $In_{1-x-y}Ga_xAl_yAs$ lattice matched to InP. *Applied Physics Letters* 1982; **41**(5): 476–478 https://doi.org/10.1063/1.93537.
21. Software spectra: TFCalc, 3.5.1 Edition. Portland, OR, 2009.
22. Cho HK, Lee JY, Kwon MS, Lee B, Baek JH, Han WS. Observation of phase separation and ordering in the InAlAs epilayer grown on InP at the low temperature. *Materials Science and Engineering B* 1999; **64**(3): 174–179 https://doi.org/10.1016/S0921-5107(99)00179-8.
23. Wolf M, Rauschenbach H. Series resistance effects on solar cell measurements. *Advanced Energy Conversion* 1963; **3**(2): 455–479.
24. Kayes BM, Nie H, Twist R, Spruytte SG, Reinhardt F, Kizilyalli IC, Higashi GS. 27.6% Conversion efficiency, a new record for single-junction solar cells under 1 sun illumination. *37th IEEE Photovoltaic Specialists Conference*, IEEE, 2011, https://doi.org/10.1109/PVSC.2011.6185831.

SUPPORTING INFORMATION

Additional Supporting Information may be found online in the supporting information tab for this article.

Pursuant to the DOE Public Access Plan, this document represents the authors' peer-reviewed, accepted manuscript. The published version of the article is available from the relevant publisher.